Proceedings of the
47th IEEE Conference on Decision and Control
Cancun, Mexico, Dec. 9-11, 2008

WeB04.4

Modeling and Identification of the Dynamics of Electrostatically Actuated Microcantilever with Integrated Thermal Sensor

Pranav Agarwal, Deepak Sahoo, Abu Sebastian, Haris Pozidis and Murti V. Salapaka

Abstract— Microcantilevers that thermally sense the topography of the sample with the ability of electrostatic actuation enable a highly parallel implementation where multiple cantilevers scan the media. Microcantilevers with integrated sensors are used for a variety of applications viz. calorimetry, thermal dip pen lithography, thermal metrology, room temperature chemical vapor deposition in addition to high density data storage application. The dynamics of these cantilevers is governed by a complex interplay of mechanical, thermal, electrostatic and interatomic forces. Such dynamics are analyzed in this paper for operating conditions that are practical for high density data storage applications ($\geq Tb/in^2$) and imaging. Models for a thermo-mechanical cantilever that are tractable for real-time applications as well as a comprehensive characterization of the relevant physical effects and methods for identifying model parameters are developed. The efficacy of the paradigm developed is proven by a comparison with experimental data.

I. INTRODUCTION

The atomic force microscope is a widely used instrument to probe and manipulate matter and its properties at atomic level. The forces on the tip due to the sample cause a deflection of the cantilever which is sensed using a laser-photodiode mechanism. However, laser based optical detection is not suitable for a highly parallel operation that may involve thousands of cantilevers (see [5], [6]). Thermomechanical levers have integrated sensing and actuation mechanism [11]. Considerable understanding of thermal sensors for topography sensing and theoretical modeling of heat conduction processes is present (see [1], [12], [4], [8], [3]). However, detailed characterization and modeling of the cantilever dynamics of an electrostatically actuated microcantilevers with integrated thermal sensors has not been done. Recently there has been considerable interest in intermittant contact mode operation using such microcantilevers (see [7], [2]). In such studies the interplay of the dynamics of the cantilever, the thermal dynamics of the reader and various forces on the tip of the cantilever have to be understood for optimizing the design, operation and interpretation of data. In levers that have integrated thermal sensing capability and actuation that is electrostatic, the related thermal and electrostatic dynamics add to the complexity of the dynamic mode operation.

In this paper, a comprehensive paradigm for characterizing and identifying tractable models for microcantilevers that incorporate solid-state means of thermally sensing topography

Murti Salapaka and Pranav Agarwal are with Department of Electrical and Computer Engineering, University Of Minnesota-Twin Cities, Minneapolis murtis@umn.edu, agar0108@umn.edu Haris Pozidis, Abu Sebastian and Deepak Sahoo are with IBM Zurich Research Laboratory, 8803 Rüschlikon, Switzerland hap@zurich.ibm.com ase@zurich.ibm.com dsa@zurich.ibm.com

that are actuated electrostatically is developed. The study incorporates the optical lever method of sensing cantilever deflection. Apart from being relevant to applications where optical sensing is available, and is used in conjunction with the thermal sensing of sample features, the optical detection provides a means to unravel the dynamics of the thermal lever. The optical lever based sensing also provides a means to calibrate the effectiveness of the models based on the thermal sensing of topography. In this paper the emphasis is on models that predict experimentally observed trajectories of the cantilever tip as sensed by the laser-photodiode mechanism. A quantitative agreement between the model predicted data and the experimentally observed trajectories is presented. The systems viewpoint to a complex interplay of physical effects with the appropriate simplifying assumptions is shown to result in a tractable means of predicting quantitatively the behavior of the system. A significant conclusion is that the model parameters can be estimated using the thermal sensor alone.

II. MODELING

Figure 1(a) shows a cantilever with the capability of sensing the distance of the cantilever from the media (also termed as the "sample") by monitoring the heat transfer to the media. The cantilever has a low doped region called thermal sensor which is connected by two highly doped legs, for the read operation. The read operation is enabled by applying a voltage V_R across the legs of the cantilever that induces a current I_R that depends primarily on the resistance of the thermal sensor. A primary mechanism of heat transfer from the cantilever is conduction to the media that depends on the separation of the cantilever and the media and this leads to a change in the resistance of the electrical path between the two legs of the cantilever. This provides the primary mechanism of topography sensing through the thermal sensor.

For the purposes of the study in this paper, the cantilever is made compatible with the Digital Instrument, Multimode Atomic Force Microscope (AFM) that has the following features (1) an optical means of detecting cantilever deflection p. (2) positioning capability with nanometer resolution, laterally (x, y direction) and vertically (z direction). In addition to the z positioning capabilities of the long range tube piezo (J-scanner), a small disc piezo, placed on the J scanner provides positioning in the z direction with a bandwidth close to 300 kHz (3) a means to electrostatically actuate the cantilever by applying a voltage V_{sub} to the sample.

The primary forces on the cantilever are (1) the tip-sample interaction force F_{ts} that is dominated by attractive forces at

large range and at short range the forces are predominantly repulsive. This force depends on the separation between the tip and the sample, t_s (2) the electrostatic force F_{esf} that is caused by the difference in potential between the tip/cantilever surface and the sample surface and depends on the lever sample separation ℓ_s (3) the Langevin thermal noise forcing.
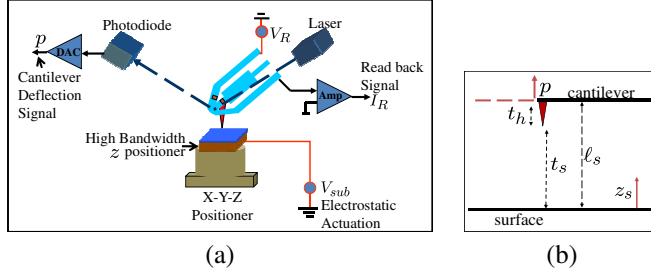

(a)   (b)

Fig. 1. (a) Experimental setup. V_R is the voltage applied across the cantilever. I_R is the measured cantilever current. V_{sub} is the voltage applied to the sample for actuating the cantilever electrostatically. Cantilever deflection is sensed through a laser-photodiode mechanism. Sample positioning is controlled through X-Y-Z positioner of DI microscope. Sample can also be positioned with high bandwidth in z direction using a high bandwidth z positioner. (b) p and z_s are the tip-deflection and the sample position respectively. t_s and t_h are the tip-sample separation and the tip height respectively. ℓ_0 (not shown) and ℓ_s is the lever sample separation.

Though an experimental means of identifying the cantilever dynamics is employed for the development of the model for dynamic mode operation purposes, the following second order approximation of the cantilever dynamics given by

$$\ddot{p} + \frac{\omega_0}{Q}\dot{p} + \omega_0^2 p = f \qquad (1)$$

where f, ω_0 and Q are the total external force, first modal resonant frequency and the quality factor of the cantilever respectively, proves useful for the approach curve analysis described later.

Before providing the modeling assumptions, notation is provided with the aid of Figure 1(b). p and z_s represent the cantilever tip deflection and sample position respectively. t_h, t_s and ℓ_0 are the tip height, the tip-sample separation and the initial distance of the lever from the sample respectively. ℓ_0 can be interpreted as the initial reference distance between the sample and a nominal point on the lever surface. The lever-sample separation ℓ_s is the instantaneous separation between the cantilever and the sample. With the above notation it follows that $t_s = l_0 + p - t_h - z_s$ and $\ell_s = \ell_0 + p - z_s$. Note that p can be measured using the laser and the photodiode arrangement and z_s can be changed by using the piezo scanner to position the sample in the vertical direction.

The modeling of the various components of the dynamics follow the principle of separating the parts of the dynamics that can be precisely characterized from the components that are either not known or are not tractable for real-time applications. Such a separation is facilitated by the feedback interconnection modeling of the various forces on the cantilever that is presented next.

A. Feedback models of tip-sample interaction forces and electrostatic forces

The cantilever tip deflection p depends on the tip-sample interaction force. The related model, denoted by G, that processes the input force to generate the deflection p is linear and does not vary with time. Also, the related cantilever dynamics can be characterized precisely [9], [13]. However, the tip-sample interaction force, that depends on the tip-sample separation t_s is non-linearly related to p and often only a qualitative nature of tip-sample force (Φ) is known. The entire dynamics can be considered as a feedback interaction of a linear time invariant system G that models the cantilever and a static nonlinearity, Φ, in the feedback path [10]. This feedback interaction model of a linear and time-invariant system with a static nonlinearity $\Phi = \frac{1}{m}F_{ts}$ is shown in Figure 2(a). The above feedback interconnection model consolidates the known information about the system G and the unknown part Φ into two separate operators that interact with each other.
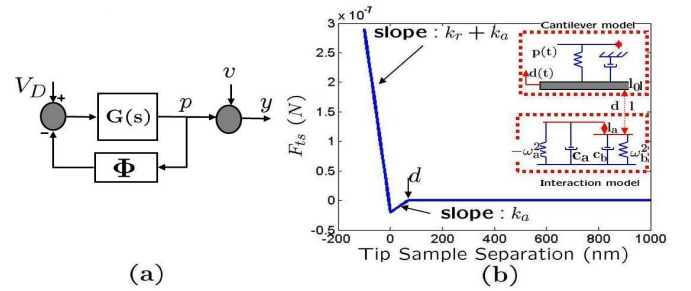

(a)   (b)

Fig. 2. (a) The feedback interconnection model encapsulates the inter-dependence of the cantilever tip-deflection p and the tip-sample interaction force F_{ts}. The cantilever is modelled as a linear time invariant system $G(s)$ that takes as the input the dither V_D and the tip-sample interaction force h (per unit mass) and provides the tip deflection p as the output. The tip-sample interaction force (per unit mass) takes as the input the tip deflection p and provides the tip-sample force per unit mass h as the output. The static nonlinearity Φ typically also depends on the tip velocity $\dot{p}$. The signal y is the photo-diode output that provides a corrupted version of the tip-deflection p with v being the measurement noise. (b) Piecewise linear model of the tip-sample interaction. k_r and k_a denote the repulsive and attractive spring constants. d is the parameter that characterizes the difference in separations between the onset of attractive and repulsive forces. d is a good measure of the thickness of the adhesion layer

A piecewise linear parametric model can be assumed to approximate the tip-sample interaction force [10]. In this model, the force on the tip is given by

$$
\begin{aligned}
F_{ts} &= 0 && \text{if } t_s > d \\
&= k_a(t_s - d) && \text{if } 0 \le t_s \le d \\
&= k_r t_s + k_a(t_s - d) && \text{if } t_s \le 0
\end{aligned}
\qquad (2)
$$

where t_s is the tip sample separation and d is a parameter that characterizes the onset of the attractive interaction. The origin is placed at the onset of the repulsive interaction (see Figure 2(b)).

The main source of inducing oscillations in the lever are electrostatic where a voltage differential is applied between the cantilever and the sample. The cantilever acts as one plate of a capacitor while the substrate forms the other plate. The cantilever feels a capacitive force denoted by F_{esf} that depends on the difference of potentials on the cantilever and

on the sample. The voltage is not uniform along the surface of the cantilever. The sample substrate can be assumed to be at V_{sub}. The cantilever surface and the substrate are modeled as a parallel plate capacitor with the voltage difference being

$$V_{esf} = \alpha_R V_R - V_{sub} \qquad (3)$$

where α_R and V_R are scaling factor and the thermal sensor voltage respectively that account for the non-uniform voltage on the cantilever surface. The capacitive (electrostatic) force on the cantilever is given by

$$
\begin{aligned}
F_{esf} &= -\frac{K_{esf}V_{esf}^2}{\ell_s^2} \quad \text{if } \ell_s > t_h \\
&= -\frac{K_{esf}V_{esf}^2}{t_h^2} \quad \text{if } \ell_s \le t_h,
\end{aligned}
\qquad (4)
$$

where V_{esf} is given by (3) and K_{esf} is the electrostatic force constant. Note that $\ell_s = \ell_0 + p - z_s$. If the lever sample distance ℓ_s is smaller than the tip height then the tip-height t_h governs the separation of the cantilever surface and the sample substrate for determining the electrostatic force on the cantilever. Figure 3(b) shows the forces felt on the cantilever

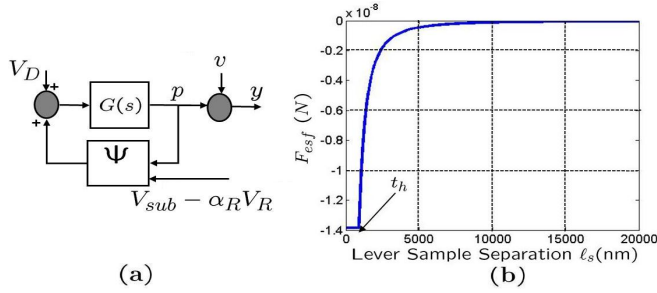**(a)**   **(b)**

Fig. 3. (a) The electrostatic force modeled by a feedback interconnection of a linear operator of the cantilever dynamics and the non-linear electrostatic force (b) Simulated electrostatic force felt by the cantilever when the lever-sample separation ℓ_s is varied.

when the lever-sample separation ℓ_s is varied. Note that the cantilever deflection affects the electrostatic force which in turn is affected by the deflection. This scenario admits a feedback interconnection as shown in Figure 3(a). The difference in the case of the electrostatic force from the tip-sample interaction force is that the electrostatic force is being introduced by the user and admits a more precise calibration than the tip-sample interaction forces that are mostly not known. However, the electrostatic force is still dependent nonlinearly on the voltage V_{sub} and the tip deflection p. As was the case with the tip-sample interaction forces, the separation of this complex nonlinear behavior from the tractable linear behavior of the cantilever is achieved in Figure 3.

The integrated model assumes that the electrostatic forces, $\Psi = \frac{1}{m}F_{esf}$, and the tip-sample interactive forces do not effect each other and can thus be modelled as additive forces on the cantilever (see Figure 4). Figure 4 illustrates how the topography, the sample profile shown as z_s, enters the model. The tip-sample separation is given by the difference between deflection p of the cantilever and the sample position z_s (modulo $\ell_0 - t_h$).

V_R and V_{sub} are voltage sources that can be provided values as desired and z_s can be changed using the piezoelectric

scanner (J-scanner) and the small piezo-disc placed on the J-scanner. The cantilever deflection p and the thermal sensor output I_R can be measured by the optical detection system and the thermal sensor respectively.

Static mode approach curves with tip-sample and electrostatic forces provide the first means of characterizing model parameters. Consider the cantilever that is experiencing a force $F(p, q)$ where p is the deflection of the cantilever and q is an independent parameter that is available as an input. For example, q can be the sample position z_s that can be changed by using the piezo positioner or it can be the electrostatic potential V_{sub} applied to the sample substrate. Assuming a one mode approximation as given in (1), it is straightforward to show that the equilibrium position p is unstable if $\frac{\partial F(p,q)}{\partial p} > k$ where k is the stiffness of the cantilever. If this condition occurs while the tip is coming closer to the sample then the tip "snaps-in" with the sample otherwise the approach is smooth. Note that in (1), the resonant frequency $\omega_0^2 = \frac{k}{m}$ where k is the spring constant of the cantilever and m is the mass of the cantilever.
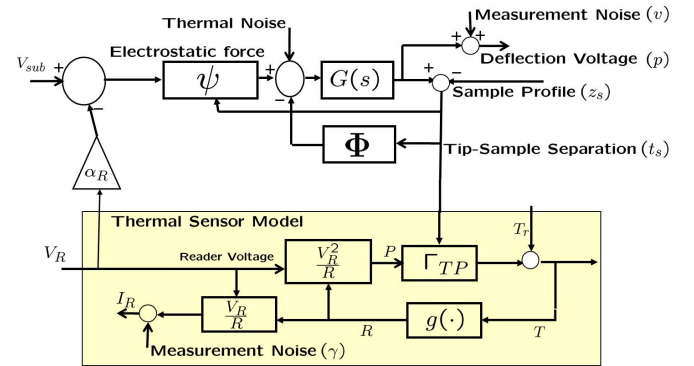

Fig. 4. Integrated systems model with a detailed model of the thermal sensing mechanism. Cantilever beam is modeled as a second order linear time invariant system $G(s)$ which takes as input the thermal noise forcing η, electrostatic force (per unit mass) F_{esf} and tip sample interaction force (per unit mass) F_{ts} and gives tip-deflection p as the output. p is measured by an optical sensor and is corrupted by a measurement noise ν. Tip sample separation $t_s = p - z_s$ modulo $(l_0 - t_h)$ is sensed by a thermal sensor which takes as input tip sample separation t_s and the thermal sensor voltage V_R and gives current I_R as the output. Measurement of I_R is corrupted by measurement noise γ

The electrostatic approach curve is obtained by using V_{sub} as the input q and recording both the optical measurement and the thermal measurement. V_{sub} is ramped up quasistatically in a linear manner and then ramped down linearly. During this process V_R is maintained at a set voltage. Note that for the electrostatic approach curve both the tip-sample interaction forces and the electrostatic forces affect the cantilever. Thus $F(p, V_{sub}) = F_{esf}(p, V_{sub}) + F_{ts}(p)$. At relatively large tip-sample separations (termed Region 1) the tip-sample interaction force is minimal and can be neglected. Assuming that the piecewise linear model (see (2)) of the tip-sample interaction force holds, if the tip-sample separation $t_s > d$ then the tip-sample interaction force is zero. In such a case, as V_{sub} is increased, the cantilever tip assumes a new

equilibrium position that satisfies

$$\begin{aligned} kp = F_{esf} & = & -\frac{K_{esf}V_{esf}^2}{\ell_s^2} \\ & = & -\frac{K_{esf}(-V_{sub}+\alpha_R V_R)^2}{(\ell_0+p)^2}. \end{aligned} \quad (5)$$

This implies that the (p, V_{sub}) pair satisfies the polynomial

$$(k)p^3 + (2\ell_0 k)p^2 + (\ell_0^2 k)p = -(K_{esf}(-V_{sub}+\alpha_R V_R)^2). \quad (6)$$

This polynomial dependence in the measured quantity p and the applied V_{sub} can be used to identify related model parameters k, ℓ_0, K_{esf} and α_R when the optical sensor is available for measuring the deflection signal p.

In a similar vein, in the region of the force curve where the tip-sample interaction forces are negligible, the equilibrium position of the cantilever also satisfies

$$\begin{aligned} -kp & = & K_{esf}\frac{(-V_{sub}+\alpha_R V_R)^2}{\ell_s^2} \\ -k(t_s + t_h - \ell_0)(t_s + t_h)^2 & = & K_{esf}(-V_{sub}+\alpha_R V_R)^2 \end{aligned} \quad (7)$$

The above is a polynomial in the data (t_s, V_{sub}) where the polynomial coefficients are dependent. Later in the paper, the relationship (7) will be used to identify parameters α_R, K_{esf}, k, t_h and ℓ_0 by utilizing the thermal sensor alone without using the optical measurement of the deflection p.

B. Model of the thermal sensor

The thermal sensor is an enabling means of detecting sample topography as it is easily integrable into a parallel operation. The laser-photodiode based detection of the cantilever deflection does not introduce any new dynamics into the system and the noise introduced by the measurement system is small. In contrast, the thermal based detection scheme measures the separation between the tip and the sample. However, the thermal sensor introduces new dynamics that is non-linear and the measurement process is more noisy than the optical based system. In this part of the paper, the models that describe the thermal sensor will be provided.

The thermal sensing scheme utilizes the change in the resistance of the lowly doped thermal sensor caused by the conduction of heat to the media which depends on the distance between the media and the cantilever. A voltage V_R is applied between the legs of the cantilever that induces a current through the cantilever. The current depends on the resistance of the lowly doped region and that in turn depends on the tip sample separation. Thus the thermal sensor is a system that is dependent on two inputs; one is the voltage V_R and another is the tip-sample separation.

1) Static parameters: First a procedure to obtain the relationship between the resistance R of thermal sensor and the temperature is presented. The primary assumption made is that for a given tip-sample separation t_s, the map between the power P and the temperature T is linear and time invariant and that the resistance R is a static, possibly nonlinear function of the temperature T. This model was first introduced in [1]. The plot of the current I_R versus V_R can be obtained (see Figure 5 (a)) by varying the voltage V_R and recording the current I_R. The resistance $R = V_R/I_R$ can be found. Figure 5 (b) shows the plot of R against V_R. Similarly,
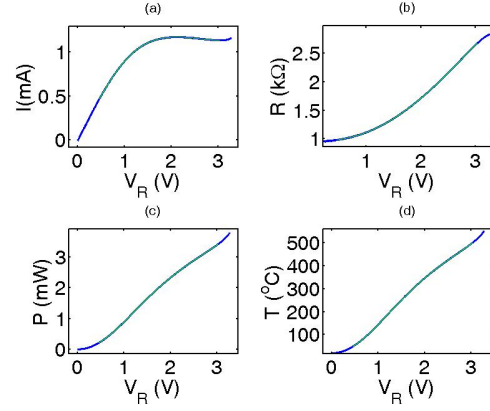

Fig. 5.　Various steps in evaluating the functional dependence $g(T)$ of resistance R on temperature T.

once R is known, the power $\frac{V_R^2}{R}$ can be evaluated. Figure 5 (c) shows the power P against V_R relationship. As the power P or the current through the thermal sensor is increased beyond a value P_k, the characteristics of the sensor change abruptly. The temperature T_k at which this breakdown of the sensor happens is a known quantity depending on the doping of the heater [1] which in the present study was calculated to be 550^0C and the power P_k at which the breakdown happens can be read from the data by recognizing the "knee" in the P vs V_R relationship. Note that the temperature at the thermal sensor is T_r (the room temperature) when the power is zero. From the above identification, the pair (T_k, P_k) is known. In the above experiment where V_R is changed in a ramp manner, the ramp input is slow. Therefore, from the linearity assumption of the power vs temperature map $\Gamma_{TP}(s)$ at a constant t_s, it follows that, the slope of the line joining $(T_r, 0)$ and (T_k, P_k) identifies $K_{TP} :=$ DC gain of Γ_{TP}. Once this information is obtained, the temperature T, at various values of V_R can be found (see Figure 5(d)). The resistance at corresponding values of V_R was found earlier and thus one can calculate the functional dependence $g(T)$ of the resistance R on temperature T.
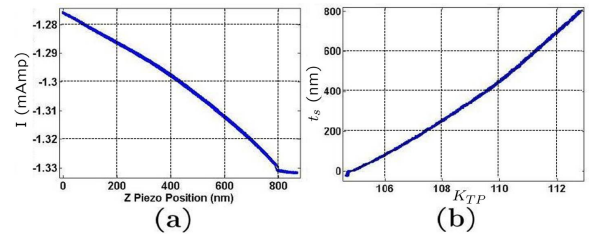

Fig. 6.　(a) The experimental z approach curve with the monitored signal being I_R. (b) K_{TP} as a function of t_s

The relationship between the power vs temperature DC gain K_{TP} and tip-sample separation t_s can be found by keeping V_R constant and performing an approach curve with z_s, the sample position, as the input and I_R as the output. Such a approach curve is shown in Figure 6(a). Note that for a given V_R and z_s, $R = \frac{V_R}{I_R}$ can be evaluated and thus

$P = \frac{V_R^2}{R}$ can be found. Also, as $g(T)$ has been evaluated in the previous section, the temperature can be found by $T = g^{-1}(R) + T_r$. Thus, the ratio $K_{TP} = \frac{T}{P}$ can be calculated at each value of z_s.

The task of converting z_s to tip-sample separation remains. An assumption is made that the value z_{s_n} of z_s at which the tip snaps into contact with the sample in the I_R vs z_s approach curve is where the tip-sample separation is zero. Another assumption made is that compared to the relevant values of z_s, the cantilever deflection p is negligibly small. These assumptions hold when the cantilever is relatively far away from the sample. With these assumptions, the sample position z_s can be converted to t_s as $t_s = z_{s_n} - z_s$. As K_{TP} is known at each value of z_s, the plot of t_s versus K_{TP} can be obtained as shown in Figure 6(b).

III. EXPERIMENTAL RESULTS

A. Model Characterization and validation using the optical based deflection measurement

The cantilever transfer function can be obtained by providing a chirp to V_{sub} and recording the deflection data p. A second order transfer function is fitted to obtain an input (V_{sub}) vs output (p) transfer function. The transfer function of the cantilever (see Figure 7) was estimated to be

$$G(s) = \frac{1.825e11}{s^2 + 1.577e5s + 2.549e11}.$$

The resonant frequency and the quality factor of the cantilever were determined to be $f_0 = 80.354$ kHz and $Q = 3.2015$, respectively.

Using the piecewise linear model (2) to fit the experimental data, the parameters k_a, k_r and d were found to be $k_a = -0.29$ N/m, $k_r = 3.4$ N/m, and $d = 65$ nm.
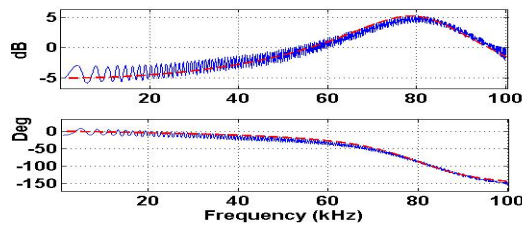

Fig. 7. A chirp signal from DC-100 kHz is applied at V_{sub} and the photodiode voltage is recorded. The input-output transfer function is estimated using Matlab. The plot shows the comparison of the estimated (red-dash) and the experimental data (blue-solid)

Figure 8(b) shows the experimentally obtained electrostatic approach curve using photodiode current as the deflection sensor. As V_{sub} is increased, the deflection follows the curve from a to b. Any further increase in V_{sub} leads to the snap-in condition where the cantilever tip makes contact with the sample at c. As V_{sub} is reduced, the cantilever snaps out of contact at d and jumps to e before retracing its path from f to a. Region 1 (a to b), corresponds to the electrostatic approach curve before snap-in occurs. The vertical axis is converted to nm by using the sensitivity S (30 nm/V) obtained using the contact mode approach curve (Figure 8(a)). If $t_s > d$ in any region of the electrostatic

approach curve, then each value of (p, V_{sub}) provides one relation (6) that is a polynomial in p with coefficients of the polynomial related. This aspect can be exploited to find the coefficients that best satisfy the relations imposed by (6). A nonlinear curve fitting algorithm based on trusted region is employed to determine a polynomial of the form (6) for the initial $a - b$ part of the approach curve where it can be assumed that tip-sample separation $t_s > d$ and therefore the cantilever experiences no interaction force. $V_R = 3V$ for the data presented. The parameters identified are $k = 0.16486$ N/m, $\ell_0 = 1318.25$ nm, $K_{esf} = 1.24 \times 10^{-21}$ F-m, $\alpha_R = 0.2085$.
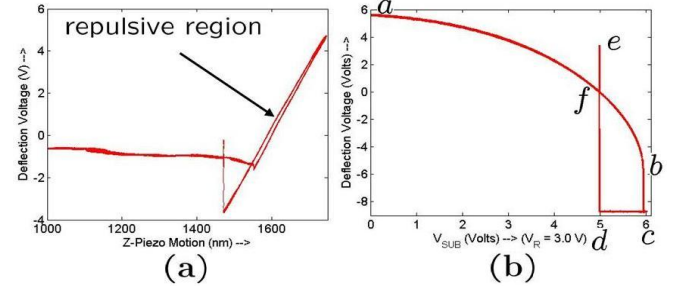

Fig. 8. (a) Experimental optical Z-Approach curve. The slope in the repulsive region is the reciprocal of the photodiode sensitivity S. (b) Experimental optical electrostatic approach curve

In this part, experimental results are compared with model-based simulation results with the model parameters as identified previously. Figure 9(a) shows the comparison of the experimentally-obtained z approach curve (piezo positioner is moved in the z direction and the deflection signal is captured) with the one obtained from the simulation model. The figure shows that the simulation model predicts the snap-in and snap-off points relatively accurately and predicts the cantilever deflection well in the repulsive region. Figure 9(b) shows the comparision of the experimentally obtained electrostatic approach curve (ramp is applied at V_{sub} and optical signal is captured) with the one obtained from the simulation model. Figure 10(a) shows the comparison between
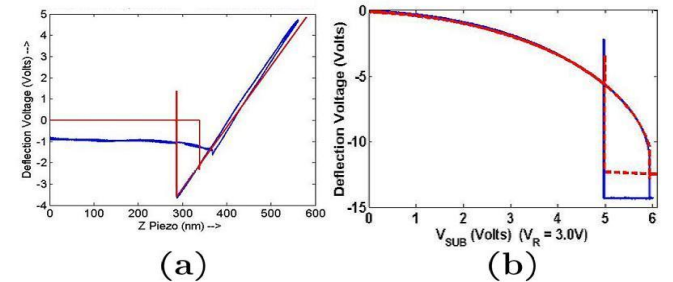

Fig. 9. (a) The experimental (blue) and model predicted (red) z approach curves are compared. (b) The experimental (blue-solid) and model predicted (red-dash) electrostatic approach curves (V_{sub} is the input and I_R is the monitored variable) are compared

experimentally measured and simulated snap off response during Z-approach curve. Exact match of frequency reveals that the cantilever model is precise enough to capture the actual resonant frequency. Figure 10(b) shows the compar-

ison between experimentally measured and simulated snap-off response during electrostatic approach curve. Exact match of frequency reveals that cantilever model also captures the reduction in resonant frequency due to electrostatic actuation.
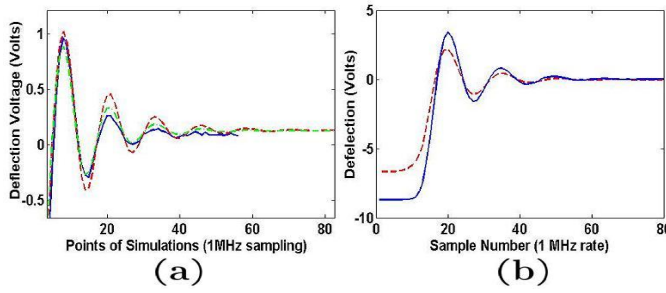

Fig. 10. (a) The experimental (blue-solid) and model predicted (red-dash Q = 3.2, green-dash Q = 2.5) snap off response in Z-approach curves are compared. (b). The experimental (blue-solid) and model predicted (red-dash) snap off response in electrostatic approach curves (V_{sub} is the input and I_R is the monitored variable) are compared.
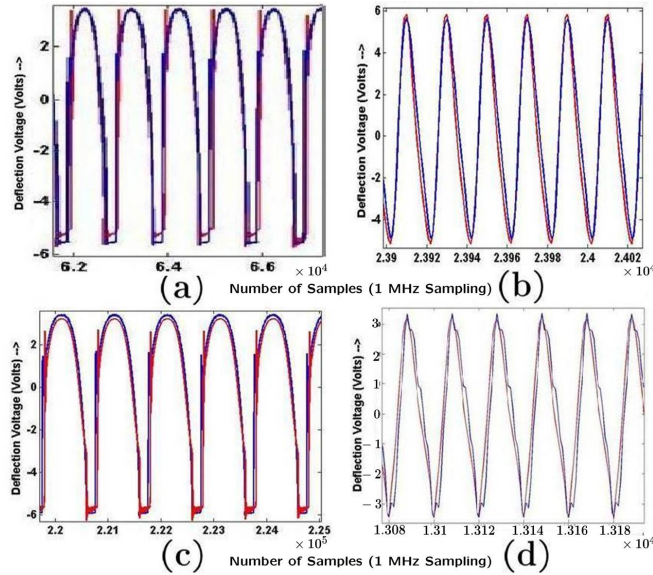

Fig. 11. (a) and (b) show model predicted data (in red-dash) and experimental results (in blue-solid) when the sample follows a square wave profile at 3 Hz with the V_{sub} following sinusoidal pattern at 1 kHz and 50 kHz. Monitored data is the photodiode signal. (c) and (d) show model predicted data (in red-dash) and experimental results (in blue-solid) when the sample follows a sinusoidal wave profile at 3 Hz (c) and 1 kHz (d) with the V_{sub} following sinusoidal pattern at 50 kHz.

Figure 11(a) shows the deflection trajectory as monitored by the optical lever when V_{sub} is a sinusoid at 1 kHz and the sample position z_s is altered in a square pattern with the square wave frequency of 3 Hz. Figure 11(b) shows the deflection trajectory as monitored by the optical lever when V_{sub} is a sinusoid at 50 kHz and the sample position z_s is altered in a square pattern with the square wave frequency of 3 Hz. These experiments are performed to evaluate the efficacy of the model in predicting the optical deflection trajectories when the tip encounters a sample profile. As is evident from the simulation and the experimental data

a quantitative match is obtained with the simulation model capable of predicting intricate features like the snap-off conditions and the response after snap-off.

Figure 11(c) shows the deflection trajectory as monitored by the optical lever when V_{sub} is a sinusoid at 1 kHz and the sample position z_s is altered in a sinusoidal pattern with the frequency of 3 Hz. Figure 11(d) shows the deflection trajectory as monitored by the optical lever when V_{sub} is a sinusoid at 50 kHz and the sample position z_s is altered in a sinusoidal pattern frequency of 2 kHz. The sample profile was discernable in the data indicating that topographic features can be read at 2000 bits/sec speeds.

B. Model characterization based on thermal sensor measurement

In most high density data storage applications, the optical means of sensing is not feasible. In this part, we present a paradigm to identify model parameters using the thermal sensor alone. An electrostatic approach curve is obtained where V_{sub} is changed in a ramp manner and I_R is recorded at the fixed V_R (see Figure 12) where the tip does not snap into contact. The I_R axis can be converted to t_s by evaluating $R = \frac{V_R}{I_R}$, $P = \frac{V_R^2}{R}$, $T = g^{-1}(R) + T_r$ and $K_{TP} = \frac{T}{P}$. Once K_{TP} is known, using Figure 6(b), t_s can be evaluated. Thus the I_R vs V_{sub} plot can be converted to t_s vs V_{sub} plot. Note that when $t_s = 0$ then any further change in V_{sub} cannot change the current I_R. Thus the value of t_s where the I_R remains constant (the part of the curve in Figure 12(b) that remains constant) should be zero. This value is approximately 20 nm instead of zero. This discrepancy, though small, is attributed to the violation of the assumptions stated earlier in section II-B.
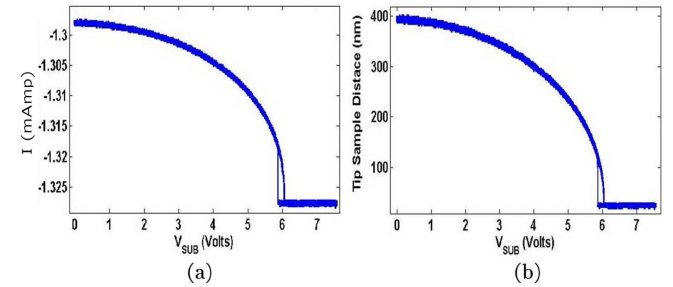

Fig. 12. (a) shows the experimental electrostatic approach curve with no snap in. (b) shows the I_R axis in (a) converted to the tip-sample separation t_s axis. This experiment was performed to check the validity of the assumptions made in converting the I_R axis to the t_s axis. The flat portion (t_s not changing with V_{sub} should be at a value of $t_s = 0$. In the plot, the portion where t_s is constant is at a value 20 nm.

1) Electrostatic Approach curve for identification: Consider an electrostatic approach curve with V_{sub} as input and I_R as the monitored variable where the tip does snap into contact with the sample substrate (see Figure 13(a)). Note that the data in Figure 13(a) can be noisy. A polynomial fit to the data is performed to obtain a clean version of the Figure 13(a) data. As indicated earlier, the I_R axis can be converted to the tip-sample separation t_s axis. Equation (7) provides a polynomial dependence of the variable t_s and V_{sub} which can be generated using the electrostatic
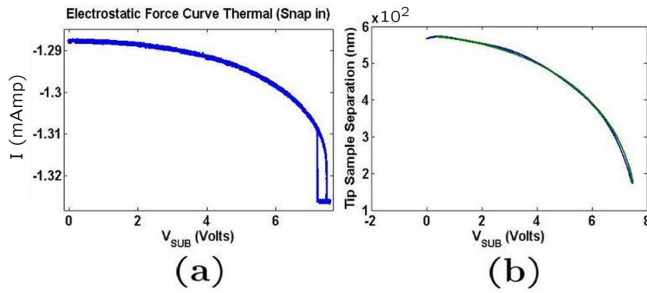
Fig. 13. Experimental electrostatic approach curve data is shown in (a). The I_R axis is converted to the tip-sample separation axis; a polynomial fit is obtained to obtain a clean version of the data. The region (Region 1) where the tip-sample interaction forces are negligible is used to identify parameters. (b) shows the parameter fit (green-dashed) and experimental data (blue-solid) in Region 1

approach curve with I_R measured and converted to t_s. A nonlinear curve fitting algorithm based on trusted region is used to identify the best fit to the data in Figure 13(b). The parameters identified are α_R, K_{esf}, k, t_h, and ℓ_0.

Estimation of mechanical cantilever parameters viz. resonant frequency and quality factor is done by fitting a second order transfer function around the resonance of transfer function from V_{sub} to I_R. This gives us an estimate of f_0 as 78.73 kHz and quality factor (Q) as 3.52.

Thus, using the above procedure a fairly good estimate of model parameters can be done using the thermal signal and actuation signal.

C. Comparison of Optical and thermal sensor based identified parameters

Parameter	Optical	Thermal
α_R	0.19	0.21
ℓ_0	1388.1 nm	1452.4 nm
K_{esf}	1.07387×10^{-21}	1.14×10^{-21}
t_h	not estimated	876.4 nm
k	0.17	0.17
f_0	77.32 KHz	78.73KHz
Q	3.46	3.52

TABLE I

There is a remarkable match between the parameters as obtained by optical detection based identification and thermal detection based identification as tabulated in Table I. This data provides evidence that the parameters needed for the model can be estimated using thermal sensor alone.

IV. CONCLUSION

This paper presents a comprehensive modelling paradigm for mechanical dynamics of cantilever with integrated thermal based sensing of topography. It also provides a precise means of identifying model parameters. The proposed methodology is corroborated with experimental data to determine the validity of the assumptions made in the modelling and identification procedures. It is evident that the systems approach to modelling the cantilever with integrated thermal sensor that interacts with the tip-sample potential and the electrostatic forces provides an efficient means of predicting

experimental data. An interesting conclusion is that the model parameters can be identified using thermal means alone. A significant outcome of the work is a simulation model that can be relied upon to be close to the experimental reality thereby obviating the need to perform elaborate experiments in evaluating various future strategies.

V. ACKNOWLEDGEMENTS

REFERENCES

[1] Sebastian A. and Wiesmann D. *To appear in proceedings of IFAC World Congress*, 2008.
[2] D.R.Sahoo, W. Häberle, P. Bächtold, A. Sebastian, H. Pozidis, and E. Eleftheriou. *Proceedings of the American Control Conference*, June 2008.
[3] W. P. King. *Journal of Micromechanics and Microengineering*, vol.15:24412448, 2005.
[4] J. Lee, T. Beechem, T. L. Wright, B. A. Nelson, S. Graham, and W. P. King. *Journal Of Micromechanical Systems*, vol. 15, No. 6:1644–1655, Dec 2006.
[5] Vettiger P., Despont M., Drechsler U., U.Dürig, W.Häberle, Lutwyche M., Rothuizen H. E., Stutz R., Widmer R., and Binnig G. *IBM J. Res. Dev.*, vol. 44, No. 3:323–340, May 2000.
[6] A. Pantazi, A. Sebastian, T. Antonakopoulos, P. Bächtold, T. Bonaccio, J. Bonan, G. Cherubini, M. Despont, R.A. DiPietro, U. Drechsler, U. Drïg, B. Gotsmann, W. Häberle, C. Hagleitner, J.L. Hedrick, D. Jubin, A. Knoll, M. A. Lantz, J. Pentarakis, H. Pozidis, R.C. Pratt, H. Rothuizen, R. Stutz, M. Varsamou, D. Wiesmann, and E. Eleftheriou. Probe-based ultra-high density storage technology. *IBM Journal on Res. and Dev.*, To be published in 2008.
[7] K. Park, J. Lee, Z. M. Zhang, and W. P. King. *Review of Scientific Instruments*, vol. 78:043709, 2007.
[8] K. Park, J. Lee, Z. M. Zhang, and W. P. King. *Journal Of Microelectromechanical Systems*, vol.16 no.2:213–222, April 2007.
[9] M. V. Salapaka, H. S. Bergh, J. Lai, A. Majumdar, and E. McFarland. *J. App. Phys.*, 81(6):2480, March 1997.
[10] A. Sebastian, M. V. Salapaka, D. Chen, and J. P. Cleveland. *Journal of Applied Physics*, 89 (11):6473–6480, June 2001.
[11] U.Drechsler, N.Burer, M.Despont, U.Dürig, B.Gotsmann, F.Robin, and P. Vettiger. *Microelectronic Engineering*, vol. 67-68:397–404, 2003.
[12] U.Dürig. *Journal of Applied Physics*, vol. 98:044906, 2005.
[13] D. A. Walters, J. P. Cleveland, N. H. Thmson, P. K. Hansma, M. A. Wendman, G. Gurley, and V. Elings. *Rev. Sci. Instr.*, 67(10):3583–3590, 1996.